Supporting Information

Modeling secondary organic aerosols from β-caryophyllene: role of extremely low-volatile organic compounds on new particle formation and evaluation of the SOA composition

Yijie Shi,*† Florian Couvidat, * Victor Lannuque, * and Karine Sartelet†

* Institut National de lEnvironnement Industriel et des Risques, INERIS, 60 550 Verneuil en Halatte, France.
† CEREA, ENPC, Institut Polytechnique de Paris, EdF R&D, IPSL, 77 455 Marne la Vallée, France.

Correspondence to: Yijie Shi (Yijie.SHI@ineris.fr)

Contents:

1 section 3 figures (Figures S1 to S3)

3 tables (Table S1 - S3)

Section 1 presents the development of the autoX-MCM mechanism, complementing the summary provided in the main text.

Table 1 summarizes the values of the optimized parameter in the developed mechanism (autoX-MCM), derived from the Cases 1-4 experiments.

Table 2 lists the fitted nucleation rate coefficient k_{nucl} for Case 5 under eight P_{sat} estimation methods, using both autoX-MCM and mMCM mechanisms. The numbers in parentheses indicate the ELVOC counts considered in each case. For each method, k_{nucl} was obtained by fitting the simulated number concentration peak to the experimental peak value[1], ensuring comparability across methods by constraining other variables. It is worth noting that for 'v1b0' and 'v1b1', the ELVOC pools are dominated by organic nitrate species, which do not participate in the nucleation of Case 5. Therefore, the corresponding k_{nucl} values should be regarded only as parameters to initiate the nucleation process and reproduce the trend in number concentration.

Table 3 compares the simulated and observed mass fractions of organic nitrate for Cases 5-7. To assess the influence of oligomerization on the organic nitrate fraction, the org-N fraction of the 'w-oligo (no oligomer N)' setup is also shown. At 298 K and 313 K, including this parameterization decreases the simulated organic nitrate fraction and brings it closer to the AMS observations of Gao *et al.* [1]. This reduction likely arises because oligomerization is restricted to organic species without a nitrate functional group (N-free), leading to a greater fraction of N-free compounds condensing into the aerosol phase.

Figure S1 compares SOA concentrations simulated with autoX-MCM under three scenarios: without oligomerization, with non-nitrate oligomerization, and with nitrate-containing oligomerization. Across all three temperature cases, the inclusion of oligomerization does not significantly affect the total SOA volume concentration. However, the non-nitrate oligomerization scenario reproduces SOA concentration that is in closer agreement with the chamber measurements of Gao *et al.* [1] than those including nitrate-containing oligomers.

Figure S2 shows the relative contributions of particle-phase oligomerization and gas-phase dimerization to oligomer formation. Across all simulated temperatures, oligomerization dominates the production of non-

nitrate oligomers, whereas gas-phase dimerization contributes mainly to nitrate-containing species.

Figure S3 illustrates the simplified and main formation pathways of β-caryophyllinic acid (BCA) during BCARY ozonolysis, which serves as a representative low-volatility product in the oxidation scheme.

1 Full autoX-MCM' reaction pathways and mechanism

1.1 O_3-initiated BCARY autoxidation scheme

1.1.1 Initiation of autoxidation

In the developed mechanism 'autoX-MCM', the initial $RO_2^{\cdot}$ species that starts the autoxidation chain is directly formed by the BCARY + O_3 reaction, such as:

$$\text{BCARY} + \text{O}_3 \longrightarrow \gamma\,\text{BCALAO}_2 + (1-\gamma)\,\text{other MCM products} \qquad k_0\ (R_0)$$

with γ being the stoichiometric coefficient of the $RO_2^{\cdot}$ (determined by fitting to chamber experimental data). The reaction R_0 is initiated by the attack of ozone on the more reactive endocyclic double bond of the BCARY, which produces a suite of products, among which the peroxy radical BCALAO2 (as named in MCMv3.3.1) is identified by Richters *et al.*[2] as a plausible candidate for initiating the autoxidation pathways. However, in the original MCMv3.3.1, the stoichiometric yield of BCALAO2 from this reaction is insufficient to account for the substantial formation of ELVOCs and SOA observed in experiments. While other structurally similar $RO_2^{\cdot}$ may also contribute to this initiation, BCALAO2 is used here as a surrogate to represent all $RO_2^{\cdot}$ undergoing autoxidation. To account for this, the yield of BCALAO2 was treated as a key adjustable parameter, denoted as γ. To ensure mass conservation across the reaction, the stoichiometric coefficients of all other original products from the BCARY + O_3 reaction were scaled proportionally so that their new sum equals (1-γ). The reaction rate constant k_0 was adopted directly from the original MCMv3.3.1 mechanism.

1.1.2 Autoxidation propagation: H−shift + O_2 addition reaction

Following the formation of the initial $RO_2^{\cdot}$ (BCALAO2), autoxidation proceeds through successive intramolecular H-shift and subsequent O_2 additions. Two propagation steps were considered sufficient to represent the dominant autoxidation pathway of BCARY initiated by ozone (R_{1a} and R_{1b}, shown in Fig.A1). This simplification is supported by experimental observations: Richters *et al.*[2] and Richters *et al.*[3] identified $C_{15}H_{23}O_6^{\cdot}$ and $C_{15}H_{23}O_8^{\cdot}$ as the most abundant highly oxygenated $RO_2^{\cdot}$ species formed via BCARY ozonolysis. Species with more than eight oxygen atoms contributed negligibly to the overall product distribution. The reaction rate constants (k_{1a} and k_{1b}) were chosen by fitting to the experimental data.

1.1.3 $RO_2^{\cdot}$ + $HO_2^{\cdot}$ reaction

In autoX-MCM, reactions between $RO_2^{\cdot}$ and $HO_2^{\cdot}$ produce hydroperoxide compounds, in which the peroxy radical group (-$OO^{\cdot}$) is replaced by a hydroperoxide functional group (-OOH). These products are generally more stable and potentially contribute to SOA formation.
For reaction R_{2a}, which describes the termination of BCALAO2 with $HO_2^{\cdot}$, the reaction products were adopted directly from the MCMv3.3.1. In contrast, the products of reactions R_{2b} and R_{2c}, $C_{15}H_{24}O_6$ and $C_{15}H_{24}O_8$, were retained as condensable species contributing to SOA formation. The reaction rate coefficients (k_{2a}, k_{2b}, and k_{2c}) were assigned the same value as the standard KRO_2HO_2 rate in MCMv3.3.1.

1.1.4 $RO_2^{\cdot}$ + NO and $RO_2^{\cdot}$ + $NO_3^{\cdot}$ reactions

Although NO and $NO_3^{\cdot}$ have different oxidation rates, they share similar mechanisms when reacting with $RO_2^{\cdot}$ radicals and tend to produce analogous products[4]. Both reactions can proceed via pathways that generate alkoxy radicals ($RO^{\cdot}$), which then undergo similar subsequent reactions. Consequently, $RO_2^{\cdot}$ + $NO_3^{\cdot}$ reactions are represented in autoX-MCM by the corresponding $RO_2^{\cdot}$ + NO mechanisms.
The primary reaction pathways for $RO_2^{\cdot}$ + NO are illustrated as follows:

$$RO_2^{\cdot} + NO \longrightarrow RO^{\cdot} + NO_2 \qquad k_3\ (SR_{a1})$$

$$RO^{\cdot} \xrightarrow{\text{H-shift + } O_2} ROHO_2^{\cdot} \qquad k_{s3}\ (SR_{a2})$$

$$ROHO_2^{\cdot} + NO \longrightarrow RO_2O_2^{\cdot} + NO_2 \qquad k_3\ (SR_{a3})$$

$$RO_2^{\cdot} + NO \longrightarrow R{=}O + NO_2 \qquad k_3\ (SR_b)$$

$$RO_2^{\cdot} + NO \longrightarrow R'{=}O + CH_3COCH_3 + NO_2 \qquad k_3\ (SR_c)$$

When $RO_2^{\cdot}$ reacts with NO, there are three pathways: as shown in reaction SR_{a1}, it is likely to form an $RO^{\cdot}$ (reaction SR_{a1}), or form a stable compound (reaction SR_b), or fragment into smaller stable compounds (reaction SR_c).

Following the PRAM model[5], the $RO^{\cdot}$ formed by reaction SR_{a1} is assumed to perform an H-shift and react rapidly with O_2 to form $ROHO_2^{\cdot}$ without competing reactions. As this reaction is instantaneous and without competition, it is not explicitly represented in autoX-MCM, and $ROHO_2^{\cdot}$ is assumed to be directly formed by reaction SR_{a1}.

Further transformation of $ROHO_2^{\cdot}$ involves either isomerization or decomposition. For $RO^{\cdot}$ species with a low oxygen content, only SR_{a1} and SR_{a3} were considered in this study, while SR_b and SR_c were neglected. This simplification is supported by Roldin *et al.*[5], who indicated that reactions SR_b and SR_c contribute negligibly under such conditions. The branching ratios among the $RO_2^{\cdot}$ + NO reaction pathways vary depending on the degree of oxygenation in the $RO_2^{\cdot}$. In this work, the branching ratios were adapted from the PRAM model and implemented within the autoX-MCM to reflect this dependency. The resulting simplified set of reactions implemented in autoX-MCM is shown in Fig.A1, including R_{3a}s, R_{3b}s, and R_{3c}.

For simplification purposes, the termination of these $ROHO_2^{\cdot}$s reaction pathways with $HO_2^{\cdot}$/$RO_2^{\cdot}$ is not explicitly included by assuming they are likely to react only with NO and $NO_3^{\cdot}$. The radicals formed from these conditions are assumed to be chemically similar to either $C_{15}H_{23}O_6^{\cdot}$ or $C_{15}H_{23}O_8^{\cdot}$ (which have one hydroperoxide group instead of two alcohol groups). While this assumption is not exact, the resulting compounds contain the same amount of oxygen and can be classified as an ELVOC in the two cases.

The kinetics of $RO_2^{\cdot}$ + NO (k_3) and $RO_2^{\cdot}$ + $NO_3^{\cdot}$ (k_4) follow the default values defined in MCMv3.3.1.

1.1.5 $RO_2^{\cdot}$ + $RO_2^{\cdot}$

Reactions between two $RO_2^{\cdot}$ radicals can lead to the formation of volatile compounds, low-volatility monomers, or dimers. In the autoX-MCM, these reactions (R_4s and R_5s) occur within the entire pool of $RO_2^{\cdot}$ present in the mechanism. Besides 119 $RO_2^{\cdot}$ species from mMCM, this pool includes the self- and cross-reactions of key species produced during the autoxidation pathway, namely $C_{15}H_{23}O_6^{\cdot}$ and $C_{15}H_{23}O_8^{\cdot}$.

To simplify the scheme, the monomeric products formed via $RO_2^{\cdot}$ + $RO_2^{\cdot}$ reactions are treated as structurally identical to those formed via $RO_2^{\cdot}$ + $HO_2^{\cdot}$ reactions. The rate constants for R_{4a}, R_{4b}, and R_{4c} reactions were determined through fitting to experimental data, as discussed in Section 2.3.3.

In addition to monomer formation, $RO_2^{\cdot}$ can also undergo dimerization to yield a single dimer species, $C_{30}H_{47}O_8$, as described in reactions R_{5a}–R_{5c}. A unified molecular structure is used to represent all dimer products for simplicity, and a single rate constant (k_8) is applied across these pathways. Although different reaction channels may produce structural isomers or compounds with varying functional groups, such differences are not expected to significantly impact the ELVOC yield in this study.

1.2 $NO_3^{\cdot}$-initiated BCARY autoxidation scheme

1.2.1 Initialization of autoxidation

Previous studies investigating HOM formation from $NO_3^{\cdot}$-initiated oxidation of several monoterpenes[6,7], identified the first-generation alkoxy radicals bearing a nitrate functional group (nitroxyl-alkoxy radicals, O_3NO-$RO^{\cdot}$) as a critical branching point at which the oxidation mechanisms of α-pinene and Δ-3-carene diverge. These studies showed that the initial nitroxyl-alkoxy radicals can undergo bond scission to yield stable compounds

(referred to as right scission) or $RO_2^{\cdot}$ (referred to as left scission), which then participate in autoxidation propagation and bimolecular reactions, ultimately forming low-volatility products consistent with observed SOA yields.

Building on the mechanisms proposed by Kurtén *et al.* [6] and Draper *et al.* [7], we assumed the same phenomenon occurs in the BCARY + $NO_3^{\cdot}$ chemistry. In MCMv3.3.1, the initial product formed from $NO_3^{\cdot}$ addition to the endocyclic double bond of BCARY is the nitroxy-alkoxy radical $C_{15}H_{24}ONO_3^{\cdot}$ (denoted as 'NBCO' in the mechanism). However, in the existing mechanism, left scission is not taken into account and NBCO leads exclusively to the formation of the volatile product $C_{15}H_{24}O_2$ (named as 'BCAL' in MCMv3.3.1), with no further radical propagation, potentially underestimating SOA formation and preventing autoxidation from occurring.

$$\mathrm{NBCO} + \mathrm{NO_3} \longrightarrow \eta\ \mathrm{C_{15}H_{24}ONO_3O_2}\cdot + (1-\eta)\ \mathrm{BCAL} + (1-\eta)\ \mathrm{NO_2} \qquad k_{n0}\ (R_{n0})$$

In this work, left scission was implemented in autoX-MCM, generating $C_{15}H_{24}ONO_3O_2^{\cdot}$ (a nitroxy-hydroperoxide peroxy radical), which enables subsequent autoxidation and ELVOC formation. Reaction R_{n0} describes the left scission, and the stoichiometric ratio of $C_{15}H_{24}ONO_3O_2^{\cdot}$ (denoted by the parameter η) governs the split between right and left scission. An initial test revealed that substantial ELVOC and SOA formation from the BCARY + $NO_3^{\cdot}$ system could only be well reproduced if this radical-forming pathway is dominant. To accurately capture the SOA yields observed in the experimental data (see Section 2.3.3), the value of η was therefore set to 1.

The reaction mechanism of $C_{15}H_{24}ONO_3O_2^{\cdot}$ was developed based on the GECKO-A mechanism generation model. The $RO^{\cdot}$ and $RO_2^{\cdot}$ formed by BCARY + $NO_3^{\cdot}$ are hereafter referred to as NO_3-$RO^{\cdot}$ and NO_3-$RO_2^{\cdot}$.

1.2.2 Autoxidation propagation: NO_3-$RO^{\cdot}$ H−shift + O_2 addition reaction

A NO_3-$RO^{\cdot}$ radical ($C_{15}H_{24}ONO_3O^{\cdot}$) is formed via bimolecular reactions between the NO_3-RO_2 formed by left scission ($C_{15}H_{24}ONO_3O_2^{\cdot}$) and NO, $NO_3^{\cdot}$, and other $RO_2^{\cdot}$ species (reactions R_{n3a} and R_{n4a}). This NO_3-$RO^{\cdot}$ can undergo autoxidation via the following reaction:

$$\mathrm{C_{15}H_{24}ONO_3O^{\cdot}} \xrightarrow{\text{H-shift + O}_2} \mathrm{C_{15}H_{24}O_2NO_3O_2^{\cdot}} \qquad \mathrm{k_{n1}\ (R_{n1})}$$

In the experimental studies focusing specifically on BCARY + $NO_3^{\cdot}$ [1], the most abundant species detected typically contained 6 to 7 oxygen atoms. Based on these observations, the autoxidation propagation in our mechanism is limited to the formation of $C_{15}H_{24}O_2NO_3O_2^{\cdot}$.

1.2.3 Bimolecular reactions

The bimolecular reactions between NO_3-$RO_2^{\cdot}$ and $HO_2^{\cdot}$, NO, or $NO_3^{\cdot}$ in the BCARY + $NO_3^{\cdot}$ system are assumed to follow the same general mechanistic principles, kinetic rates, and simplification strategies as their analogues in the BCARY + O_3 scheme (see Sec. 1.1.3 Sec. 1.1.4). The overall mechanism is illustrated in Fig.A2.

In addition, NO_3-$RO_2^{\cdot}$ may further react with the $RO_2^{\cdot}$ pool (reactions R_{n4a} and R_{n4b}). Consistent with the O_3-initiated BCARY ELVOC formation mechanism, these NO_3-$RO_2^{\cdot}$ + $RO_2^{\cdot}$ reactions involve multiple types of $RO_2^{\cdot}$, including the NO_3-$RO_2^{\cdot}$ radical generated during the autoxidation in the BCARY + $NO_3^{\cdot}$ system and 121 $RO_2^{\cdot}$ species described in Sec. 1.1.5. Such reactions can yield more oxidized NO_3-$RO_2^{\cdot}$ intermediates or stable products with –OOH, -OH, and =O functionalities. For reaction R_{n4a}, GECKO-A predicts the formation of a NO_3-$RO^{\cdot}$ with a high stoichiometric yield (60%), along with semivolatile stable products that can lead to SOA formation, including $C_{15}H_{25}ONO_3O$ and $C_{15}H_{23}ONO_3O$. For NO_3-$RO_2^{\cdot}$ species derived from the H-shift reaction ($C_{15}H_{24}O_2NO_3O_2^{\cdot}$), the products of reaction R_{n4b} are treated analogously to those produced from NO_3-$RO_2^{\cdot}$ + NO/$NO_3^{\cdot}$ pathways (reactions R_{n3a} and R_{n3b}), due to their structural similarity. For NO_3-$RO_2^{\cdot}$ + $RO_2^{\cdot}$ dimerization (reactions R_{n5a} and R_{n5b}), the number of nitrate groups present in the dimers depends on the reacting $RO_2^{\cdot}$. For simplification purposes, all dimers are presented with a single nitrate group and the same structure. The rate constants are set equal to those for $RO_2^{\cdot}$ + $RO_2^{\cdot}$ reactions in BCARY + O_3 mechanism (k_{n4} = k_5 and k_{n5} = k_8).

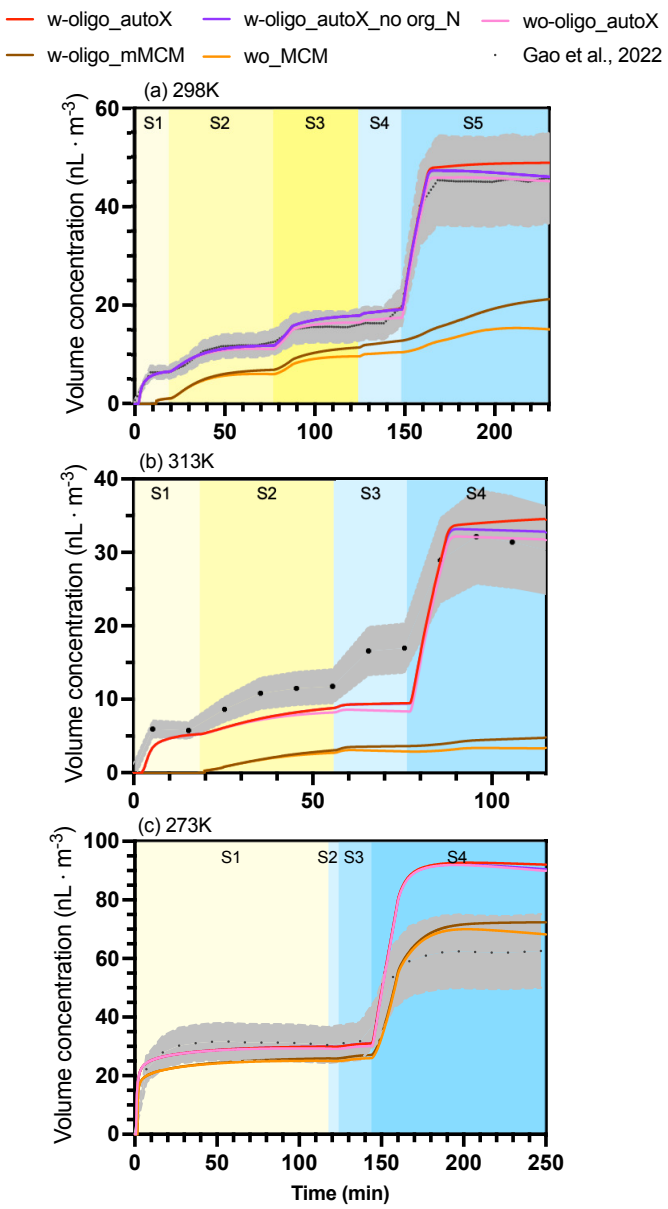

Figure S1. Modelmeasurement comparison for Cases 5-7 (BCARY oxidation at (a) 298 K and (b) 313 K, respectively) simulated with different scenarios of autoX-MCM. The measurements of the chamber are shown by a dotted black line and a gray shadow indicating the error range.

Table S1. Result of constraints in autoX-MCM. The unit of kinetic rates is s^{-1}.

Constrained Parameters	Formula or values
γ	0.0483
k_{1a}	2.0×10^{18} × exp(-1.2077×10^4/TEMP)
k_{1b}	3.0×10^{17} × exp(-1.2077×10^4/TEMP)
k_5	3.0×10^{-11}
k_6	1.26×10^{-10}
k_7	2.0×10^{-11}
k_8	1.575×10^{-11}
η	1.00

Table S2. Fitted nucleation rate coefficients ($particles\mu g^{-2}m^3s^{-1}$) for Case 5 (298 K) derived under different P_{sat} methods using the autoX-MCM and mMCM mechanism; the number of ELVOCs of each condition is listed in the parentheses.

P_{sat} estimation method	autoX-MCM	mMCM
evap	3.70E-07 (9)	1.35E-07 (6)
sim	4.33E-07 (12)	1.85E-05 (9)
v0b0	3.59E-07 (16)	1.53E-07 (13)
v0b1	3.74E-07 (15)	5.30E-06 (11)
v0b2	4.52E-07 (119)	4.70E-07 (111)
v1b0	1.65E-07 (1)	no ELVOC (0)
v1b1	4.00E-07 (2)	no ELVOC (0)
v1b2	4.87E-07 (50)	2.80E-07 (42)

Table S3. Modelmeasurement comparison for Case 5-7: the mass fraction (%) of organic nitrate in total organic. * (no oligomerization org-N)

Cases	mMCM	autoX-MCM	w-oligo_auto	Gao *et al.* [1] (AMS)
273 K 6b	21.88	41.65	41.13	35.79
298 K 5b	28.50	62.00	58.07	58.96
313 K 7b	21.37	70.30	66.98	61.06

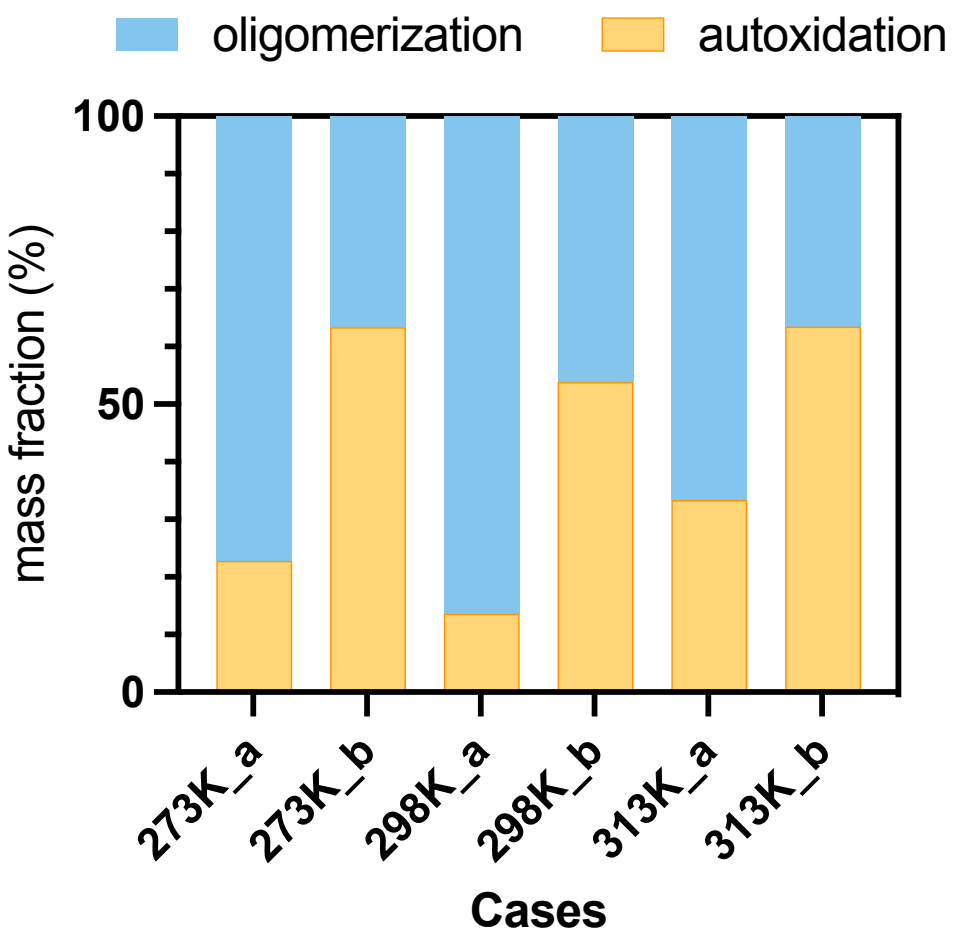

Figure S2. Contribution in (%) of particle-phase oligomerization and gas-phase dimerization in the oligomer formation (oligomerization of Org-N is not considered in this simulation). The oligomer was separated into 'autoxidation'(dust yellow) and 'oligomerization'(iceberg blue) pathways.

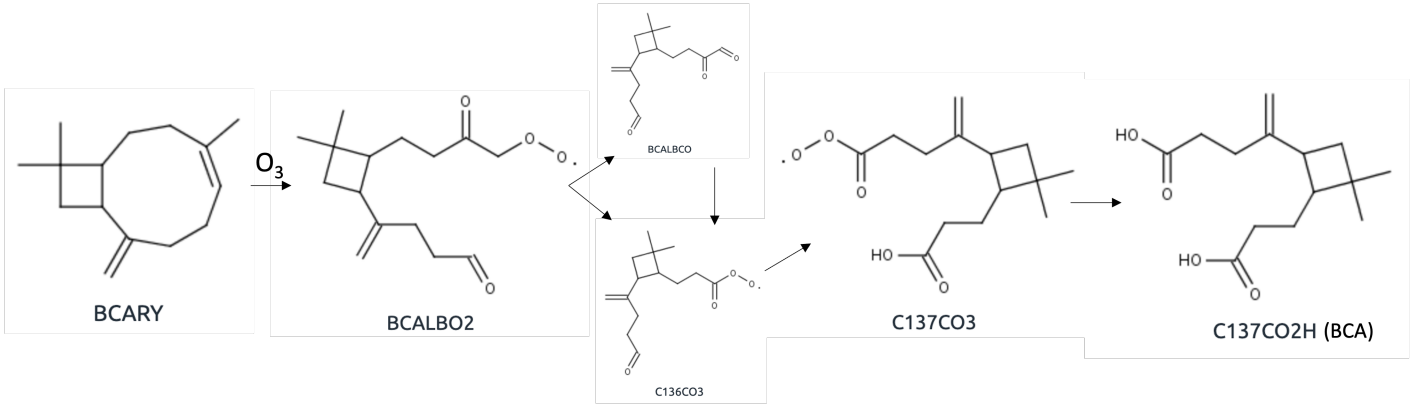

Figure S3. The main pathways of BCA formation in BCARY ozonolysis.

Notes and references

[1] L. Gao, J. Song, C. Mohr, W. Huang, M. Vallon, F. Jiang, T. Leisner and H. Saathoff, *Atmospheric Chemistry and Physics*, 2022, **22**, 6001–6020.

[2] S. Richters, H. Herrmann and T. Berndt, *Atmospheric Chemistry and Physics*, 2016, **16**, 9831–9845.

[3] S. Richters, H. Herrmann and T. Berndt, *Environmental science & technology*, 2016, **50**, 2354–2362.

[4] R. Atkinson and J. Arey, *Chemical reviews*, 2003, **103**, 4605–4638.

[5] P. Roldin, M. Ehn, T. Kurtén, T. Olenius, M. P. Rissanen, N. Sarnela, J. Elm, P. Rantala, L. Hao, N. Hyttinen, L. Heikkinen, D. R. Worsnop, L. Pichelstorfer, C. Xavier, P. Clusius, E. Öström, T. Petäjä, M. Kulmala, H. Vehkamäki, A. Virtanen, I. Riipinen and M. Boy, *Nature communications*, 2019, **10**, 4370.

[6] T. Kurtén, K. H. Møller, T. B. Nguyen, R. H. Schwantes, P. K. Misztal, L. Su, P. O. Wennberg, J. L. Fry and H. G. Kjaergaard, *The Journal of Physical Chemistry Letters*, 2017, **8**, 2826–2834.

[7] D. C. Draper, N. Myllys, N. Hyttinen, K. H. Møller, H. G. Kjaergaard, J. L. Fry, J. N. Smith and T. Kurtén, *ACS Earth and Space Chemistry*, 2019, **3**, 1460–1470.